Provided for non-commercial research and education use.
Not for reproduction, distribution or commercial use.

This article appeared in a journal published by Elsevier. The attached copy is furnished to the author for internal non-commercial research and education use, including for instruction at the authors institution and sharing with colleagues.

Other uses, including reproduction and distribution, or selling or licensing copies, or posting to personal, institutional or third party websites are prohibited.

In most cases authors are permitted to post their version of the article (e.g. in Word or Tex form) to their personal website or institutional repository. Authors requiring further information regarding Elsevier's archiving and manuscript policies are encouraged to visit:

http://www.elsevier.com/copyright

Author's personal copy

ELSEVIER

Available online at www.sciencedirect.com
ScienceDirect

Journal of Non-Crystalline Solids 354 (2008) 3025–3033

JOURNAL OF NON-CRYSTALLINE SOLIDS

www.elsevier.com/locate/jnoncrysol

Electronic structure and charge transport properties of amorphous Ta_2O_5 films

V.A. Shvets [a], V.Sh. Aliev [a], D.V. Gritsenko [a], S.S. Shaimeev [a], E.V. Fedosenko [a], S.V. Rykhlitski [a], V.V. Atuchin [a], V.A. Gritsenko [a], V.M. Tapilin [b], H. Wong [c,*]

[a] *Institute of Semiconductor Physics, SB RAS, Novosibirsk 630090, Russia*
[b] *Institute of Catalysis, SB RAS, Novosibirsk 630090, Russia*
[c] *Department of Electronic Engineering, City University of Hong Kong, Tat Chee Avenue, Kowloon, Hong Kong*

Received 6 September 2007; received in revised form 27 November 2007
Available online 4 March 2008

Abstract

Amorphous Ta_2O_5 films were deposited by sputtering Ta onto silicon substrates with reactive ion beam. Electron energy loss spectroscopy measurements on the film found that the plasma oscillation energy is 23.1 eV. The refractive index and the extinction coefficient were measured with spectroscopic ellipsometry over the spectral range of 1.9–4.9 eV. The optical band gap is found to be 4.2 ± 0.05 eV. The valence band consists of three bands separated by ionic gaps. The values of electron effective masses were estimated with DFT quantum-chemical calculation. Experiments on injection of minority carriers from silicon into oxide were also conducted and we found that the electron component of conduction current governed by the electron current in the amorphous Ta_2O_5.
© 2008 Elsevier B.V. All rights reserved.

PACS: 68.49.Uv; 71.15.Mb; 71.20.−b; 72.20.−i; 78.20.−e

Keywords: Band structure; Dielectric properties, relaxation, electric modulus; Ellipsometry; Atomic force and scanning tunneling microscopy; Ab initio; XPS

1. Introduction

As the amorphous tantalum pentaoxide (Ta_2O_5) film possess high thermodynamic stability and with large refractive index of 2.1, it was used as antireflection coating for silicon solar cells and used in the multilayer interference filters and other optical devices [1]. Recent intensive investigations focus on the applications of this film in dynamic random access (DRAM) capacitors [2–4]. Meanwhile, the reduction of gate dielectric thickness in metal-oxide-semiconductor (MOS) structures has prompted the search for higher dielectric constant (high-k) oxide materials to replace the traditional SiO_2 ($k = 3.9$) and Si_3N_4 ($k = 7$) [5,6]. Among the high-k materials, Ta_2O_5 films received considerable attention because of its high dielectric constant ($k = 25$). Besides this, high-k materials may be used as blocking dielectric in a gate stack of flash memory devices [7]. In this article, we investigate physical and electrical properties of amorphous Ta_2O_5 films prepared by ion-beam sputtering deposition (IBSD) method. We shall focus on the electronic structure and the electrical characteristics of this oxide. Polycrystalline Ta_2O_5 films are used in DRAM for better charge storage and the current leakage is crucial for this application. It is well known that the leakage current is governed Fowler–Nordheim (FN) tunnel mechanism and the effective mass of carrier is one of the most important parameters. In this work, we determined, for the first time, the carrier effective masses in Ta_2O_5 using quantum-chemical simulation. On the other hand, the charge transport in Ta_2O_5 films can be contributed by either electrons or holes. To have a better understanding of the charge transport properties, separation of the electron and hole currents are also important. The work also

* Corresponding author. Tel.: +852 27887722; fax: +852 27887791.
E-mail address: heiwong@ieee.org (H. Wong).

0022-3093/$ - see front matter © 2008 Elsevier B.V. All rights reserved.
doi:10.1016/j.jnoncrysol.2007.12.013

Author's personal copy

conducted experiment to separate these currents. In addition, the optical constant dispersions of Ta_2O_5 films are also studied, for the first time, using spectroscopic ellipsometry.

2. Experimental details

The tantalum pentaoxide (Ta_2O_5) films were prepared by ion-beam sputtering deposition system illustrated in Fig. 1. The deposition chamber was initially evacuated by turbo molecular pump to a residual pressure of 2×10^{-5} Pa. This chamber is equipped by Kaufmann ion source (1) with ion-beam diameter of 6 cm. The target used for the deposition was tantalum with 99.95% purity (2). Tantalum disc sputtering was produced by Ar^+ beam with ion energy of 1200 eV and current density of 1.2 mA/cm^2. During the film deposition the substrate temperature was maintained at lower than 70 °C. The tantalum atoms reacted with oxygen atoms from the oxygen source (3) and deposition on the substrate (4). The film thickness is monitored with a quartz crystal microbalance (5). The system equipped with additional lock-chamber (6) with RF plasma cleaning system (7). During the deposition the pressure was changed to about 1.5×10^{-2} with the inlet of gas mixture with Ar/O_2 ratio of 2. The (1 0 0) Si wafers with resistivity of about 5–7 Ω cm were used as the substrates. Just before the insertion of the substrate into the chamber, the native oxide of the substrate was removed HF etching. In several experiments the substrates were subjected to supplementary surface treatment in lock-chamber by low energy Ar^+ ion bombardment.

The crystallographic properties of the Ta_2O_5 films were controlled by a reflection high-energy electron diffraction (RHEED) at an electron accelerating voltage of 50 kV. A charge neutralization flood gun was utilized to eliminate charging effects. Top surface chemical composition and electronic parameters of the oxide films were determined by Riber LAS 3000 X-ray photoelectron spectroscopy (XPS) with monochromatic Al K_α ($h\nu = 1486.6$ eV) excitation source. Electron energy loss spectra (EELS) were measured using the same spectrometer. Bandgap of the tantalum pentaoxide film was measured by EELS using monochromatic electron beam with energy of 200 eV.

The surface morphology of the films was studied with a Solver P47 H atomic force microscopy (AFM). This microscope provides a lateral and depth resolutions of 15 nm and 0.05 nm, respectively. The AFM images were generated in resonance frequency of 150 kHz in semi-contact mode with platinated cantilever.

Spectroscopic ellipsometry measurements were carried out using an instrument operating at a balance configuration and Xe lamp was used as a light source. The spectrum ranging from 1.9 to 4.9 eV and has a resolution of 0.05 eV. The incident angle was fixed at 70.6°. Ellipsometric surface mapping was performed on LEF-8 MICROSCAN single-wavelength ($\lambda = 632.8$ nm) instrument equipped with specially designed micro-objective and stepper-motor-driven scanning stage. In-plane resolution of the map was determined mainly by the size of the focused laser beam (ellipti-

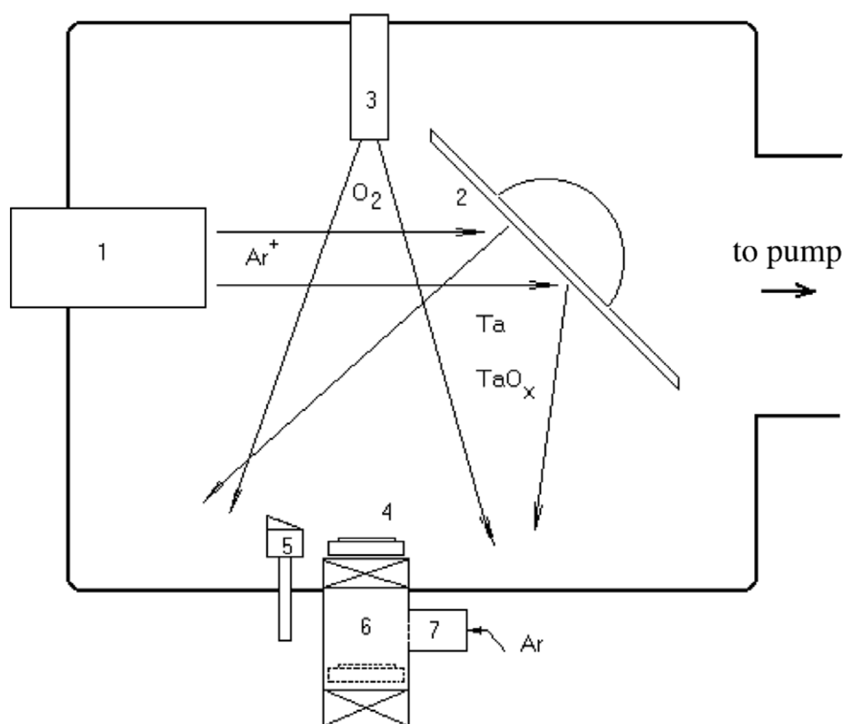

Fig. 1. Set up for reactive ion deposition. The components are: 1 – ion source, 2 – tantalum target, 3 – oxygen source, 4 – substrate, 5 – quartz crystal microbalance, 6 – lock-chamber, 7 – high-frequency input.

Author's personal copy

cal) spot on the sample surface, which could be as small as 3 μm × 10 μm. Built-in software was adopted to display the ellipsometric data and to calculate film parameters (refractive index, n and extinction index, k) during the scanning.

The metal-insulator-semiconductor (MIS) structures Si/Ta_2O_5/Al fabricated on Si(100) substrates of n- and p-type with bulk resistance of about 10 Ω cm. The Ta_2O_5 film thickness was in the range of 30–60 nm. Current–voltage and capacitance–voltage characteristics measurements were conducted at room temperature. Some measurements were conducted with tungsten lamp illumination.

3. Structure, morphology and chemical composition

Fig. 2 shows the RHEED pattern of a typical tantalum oxide film. A superposition of single crystal streaks and diffused hallo is found. Structural analysis reveals that the streak pattern should be attributed to Si(100). These streaks are generated by some regions that free of oxide. The tantalum oxide film should be mainly amorphous. Fig. 3 shows 2-D AFM image and statistical analysis of typical tantalum oxide film. The surface roughness is in the range of 0.3–0.4 nm that is very close to averaged bond length of Ta–O (0.205 nm) in crystalline Ta_2O_5 [8]. The surface morphology was further confirmed with ellipsometry measurements. The distributions of thickness and refractive index from the ellipsometry measurements are shown in Fig. 4. From the maps it can be seen that the film has very uniform thickness (d) with relative variation as low as $\Delta d/d < 0.1\%$. The relative variation of refractive index (n) is determined as $\Delta n/n < 2.4\%$.

XPS measurement on the bonding structure of Ta_2O_5 was performed. Chemical composition of the film was determined using the detailed spectra of Ta 4f doublet and O 1s core level. The Ta/O element ratio is about 0.4 with possible error of about 3%. This finding confirms that

Fig. 2. RHEED pattern of Ta_2O_5/Si film.

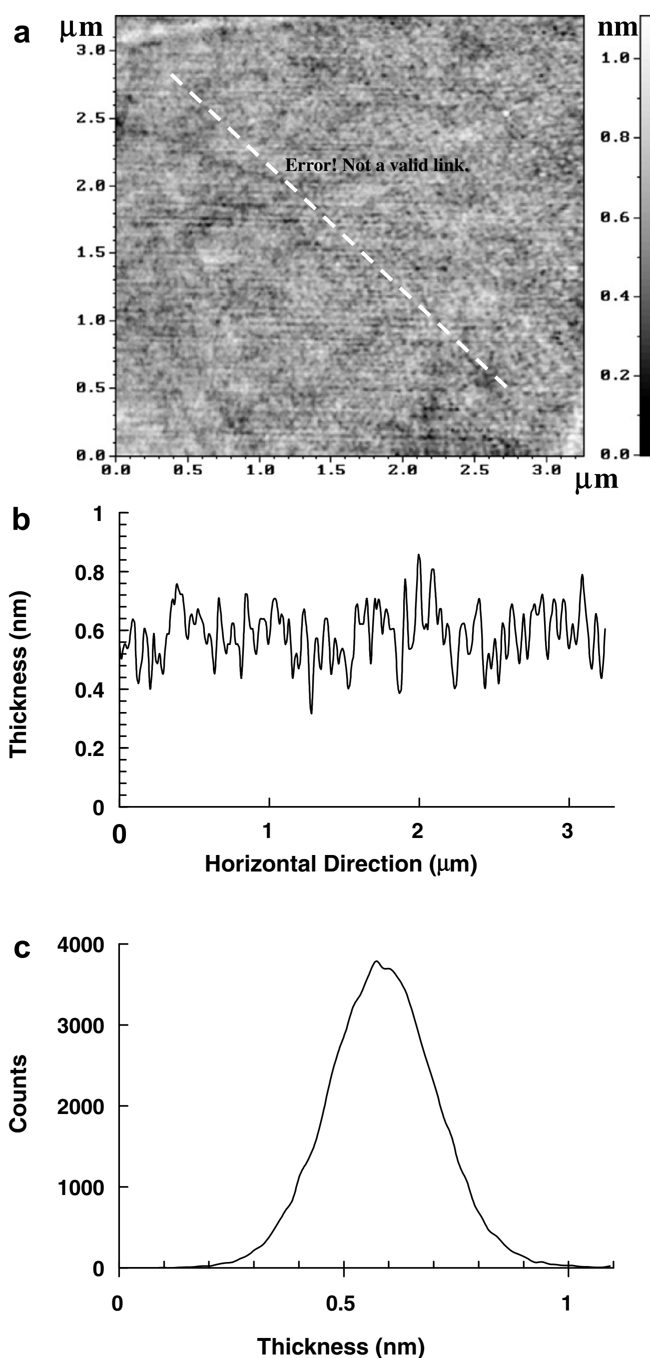

Fig. 3. Surface morphology of as-deposited Ta_2O_5 film. (a) AFM image, (b) surface roughness profile along AB line, and (c) thickness distribution profile.

the as-deposited Ta_2O_5 film is stoichiometric. Binding energies (BE) of Ta $4f_{7/2}$ and O 1s lines measured in our experiment are listed in Table 1 together with available literature results obtained earlier for Ta_2O_5 films fabricated by different methods. The scattering of published BE values for Ta $4f_{7/2}$ and O 1s lines is as high as 1.0 eV and 1.3 eV, respectively; that is larger that the possible instrumental error of photoelectron energy determination. This large deviation should be due to, at least partly, the variation in nature

Author's personal copy

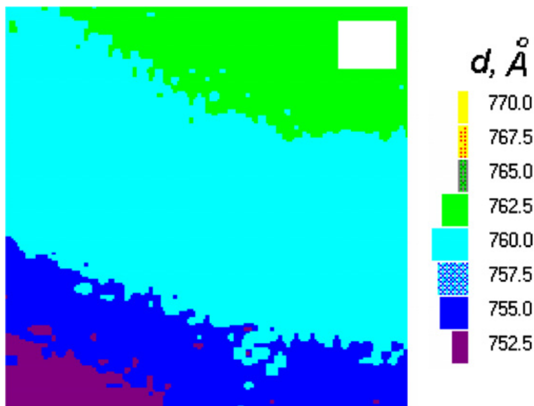

Fig. 4. Thickness (a) and refractive index (b) maps of Ta_2O_5 film over a scanning area of $4 \times 4\ mm^2$.

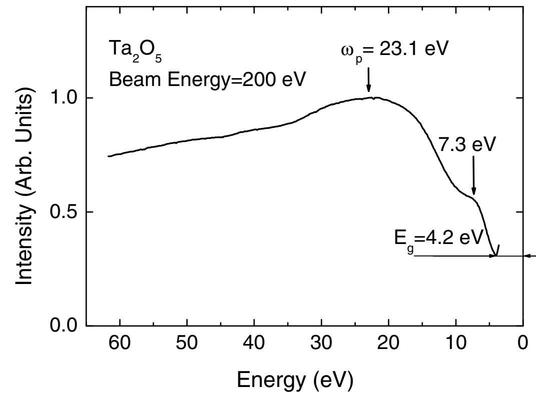

Fig. 5. Electron energy loss spectra of the as-deposited Ta_2O_5 film.

of adventitious hydrocarbon in different XPS devices [9]. This factor is able to generate a drastic shift of C 1s core level BE which was employed for charging referencing at the dielectric surface. The effect, however, can be greatly suppressed by using binding energy difference ΔBE = -BE(O 1s) – BE(Ta $4f_{7/2}$) for the characterization of Ta–O bonding. This method was successfully applied for the comparative analysis of some complex oxide crystals [10–13]. Based on this method, the deviation of ΔBE values can be reduced to as low as 0.7 eV (see Table 1). The ΔBE value found in our experiment agree well with those reported in the literatures. In some studies the crystallinity of Ta_2O_5 films were taken into account for variation of the ΔBE values because of the different atomic ordering in tantalum oxide. ΔBE in the range of 504.1–504.5 eV were obtained for crystal tantalum pentaoxide phases. Larger values (504.6–504.7 eV) were found in amorphous Ta_2O_5 because of longer Ta–O bond length in amorphous phase. Similar relations between ΔBE and bond length were reported for Nb–O and Ti–O bonds [10,11].

4. Plasma oscillations of valence electrons

Electron energy loss spectrum in amorphous Ta_2O_5 is presented in Fig. 5. The band with maximum at $\hbar\omega_B = 23.1$ eV is attributed to the plasma oscillations of valence electrons. The shoulder at energy of about 7.3 eV is due to the electron transitions from valence band into conduction band. The bandgap of the amorphous Ta_2O_5 can be estimated from the low energy threshold at 4.2 eV.

The plasma oscillation frequency (ω_p) of free electron is governed by

$$\omega_p^2 = \frac{4\pi Ne^2}{m}, \qquad (1)$$

where N is the concentration of the valence electrons involved in the plasma oscillations, m and e are mass and charge of electron, respectively. Theoretical energy of plasma oscillations calculated with using (1) is 23.2 eV which is very close to experimental value.

Table 1
Binding energies of core levels for the constituent element in Ta_2O_5 films

BE (Ta $4f_{7/2}$) (eV)	BE (O 1s) (eV)	Charging Ref., line and BE	ΔBE (eV)	Film structure	Source
27.1	531.8	C 1s, 285.0	504.7	Amorphous	[14]
26.4	530.9	O 1s, 530.9	504.5	Crystalline	[15]
26.2	530.5	–	504.3	Crystalline	[16]
26.3	530.7	C 1s, 285.0	504.4	–	[17]
26.4	530.5	C 1s, 285.0	504.1	–	[18]
26.6	531.4	C 1s, 285.0	504.8	–	[19]
26.6	530.9	–	504.3	Crystalline	[20]
27.2	531.3	C 1s, 285.0	504.1	Crystalline	[21]
26.0	530.6		504.6	Amorphous	This study

5. Spectroscopic ellipsometry

In the framework of a three-layer (ambient-film-substrate) model, the dependence of ellipsometric parameters Ψ and Δ of the system can be symbolically expressed as [22,23]

$$\tan \Psi e^{i\Delta} = F(n, k, d, E, n_s, k_s), \qquad (2)$$

where n_s and k_s are the refractive index and extinction coefficient of the Si substrate; d is the dielectric thickness and E is the photon energy. To extract the optical constants of Ta_2O_5 film (n and k), Eq. (2) was solved numerically for each wavelength. Silicon optical constants used in the calculation were taken from [24] and an estimated dielectric layer thickness was used as an initial value. For photon energies less than 4.0 eV, the film is transparent and $k = 0$. This criterion was used as a constraint for further iteration.

Fig. 6 shows the calculated extinction coefficient for Ta_2O_5 film with estimated thickness of 70, 74 and 78 nm. It can be seen that the best result is achieved when $d = 74$ nm. However, it is also seen for $\hbar\omega < 3.4$ eV that the $k(\hbar\omega)$ value is non-zero for all calculations. These deviations are most pronounced at 3.4 and 4.2 eV where critical points E_1 and E_2 in the optical spectrum of the silicon substrate are located (indicated by arrows in Fig. 6). It was shown by Arwin and Aspnes [25] that this kind of artifacts

Author's personal copy

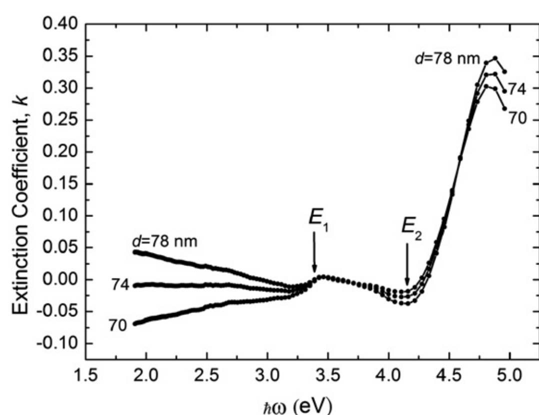

Fig. 6. Calculated extinction coefficient for precise thickness determination. The best result was achieved when $d = 74$ nm.

are most likely induced by the inadequacy of the optical model used (three-layer in our case) in approximating the real sample structure. A better approximation is to include the SiO_2 interlayer between the Ta_2O_5 and Si substrate. This approach does improve the accuracy by moving the calculated $k(\hbar\omega)$ curve toward the $k = 0$ axis (i.e. in the right direction) for $3.5 < \hbar\omega < 4.3$ eV. No significant improvement can be found for $\hbar\omega < 3.4$ eV, however.

It is seen for $\hbar\omega > 4.3$ eV that the extinction coefficient of the film increases sharply which implies the occurrence of interband absorption in Ta_2O_5. At energy of 4.8 eV we observed a broad maximum in the extinction coefficient. This peak is related to the singularity in the Ta_2O_5 interband density of states. The spectral dependence of absorption coefficient α is a function of energy. In wide gap amorphous solids, it is described by the Tauc equation [26]

$$\alpha = B\frac{(\hbar\omega - E_g)^2}{\hbar\omega}, \quad (3)$$

where B is a constant depending on the density of states in the valence and conduction bands; E_g is the optical band gap. Extrapolation of straight line in $\sqrt{\alpha\hbar\omega} - \hbar\omega$ plot yields an optical gap of 4.2 ± 0.05 eV. This value agree with the published Ta_2O_5 experimental gap values of 4.3 eV [27] and the theoretical estimated value of 4.4 eV [28]. The spectral dependence of Ta_2O_5 refractive index $n(\hbar\omega)$ is shown in Fig. 7. The refractive index increases from 2.1 at $\hbar\omega = 2.0$ eV up to 2.9 at $\hbar\omega = 4.7$ eV. It is well known that the refractive index gets larger when tantalum pentoxide becomes metal-rich [27]. Compared to Demiryont, Sites and Geib's data [27], it is confirmed again that our Ta_2O_5 films is stoichiometric.

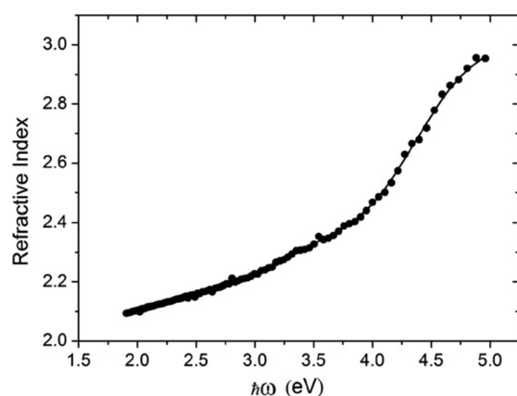

Fig. 7. Typical spectral dependence refractive index of as-deposited Ta_2O_5 film.

6. Electronic structure revealed by DFT calculation

To understand the electronic structure of tantalum pentaoxide and to estimate the electron and hole effective masses, density functional theory (DFT) calculations were performed. The calculations were performed in the framework of DFT with local density approximation (LDA). Ultrasoft pseudo-potentials were used for core electrons. Among the Ta_2O_5 different polymorphs, the orthorhombic phase which contains 22Ta and 55O atoms in the unit cell is the most stable one [29]. All Ta atoms of the unit cell are located at a plane with lattice vectors with $a = 0.6198$ nm and $b = 4.029$ nm. In the following we will refer to the Ta–O plane that containing 33O atoms. The Ta–O planes in the crystal lattice are separated by vector $c = 0.3888$ nm. The rest 22O atoms of the unit cell are located between Ta atoms of neighboring planes. These O atoms build up a plane which will be referred as O plane. It is not easy to calculate the electronic structure of a crystal with such a big unit cell and usually simplified models of Ta_2O_5 structure were used in the calculations [30,31]. A geometry optimized Ta_6O_{15} unit cell was used in Ref. [30] to simulate the non-defect containing electronic structure. Simplified Ta_4O_{10} unit cell was also used [31]. These simplified unit cells keep the local environment of Ta atoms close to that of the real unit cell where Ta atoms has five or four neighboring O atoms in the Ta–O planes.

In present calculations, Ta_4O_{10} fragment of the unit cell with or without geometry optimization were used. The atom positions in the Ta–O plane are listed in Table 2. We found that the optimized positions do not have significant difference with those in the real unit cell. Nevertheless, we would like to point out the peculiarity of relaxed unit

Table 2
Atomic positions in Ta–O plane for non-optimized (in brackets) and optimized unit cell (in unit of $a = 11.7164$ a.u.)

Atom	x	y
Ta1	0.008 (0.000)	0.010 (0.000)
Ta2	0.063 (0.065)	0.583 (0.530)
Ta3	0.517 (0.522)	0.890 (0.895)
Ta4	0.554 (0.549)	0.299 (0.300)
O1	0.677 (0.648)	−0.011 (0.000)
O2	0.279 (0.251)	0.150 (0.188)
O3	0.887 (0.882)	0.307 (0.297)
O4	0.393 (0.402)	0.579 (0.600)
O5	0.792 (0.798)	0.740 (0.709)
O6	0.185 (0.189)	0.898 (0.880)

Author's personal copy

cell. The atom positions in Ta–O plane of non-relaxed unit cell are shown in Fig. 8. Enrollment of Ta atoms being coordinated by 5 or 4O atoms depends on the position of O atoms. For example, the distance between Ta3–O20 is 0.339 nm, while the distance between O20–Ta10 is 0.258 nm. The distances for O11–Ta6 and O11–Ta9 are 0.297 and 0.319 nm, respectively. According to these distances we refer Ta6 and Ta10 to fivefold coordinated and Ta3 and Ta9 to fourfold coordinated positions. The relaxation shifts all O atoms, like O11 and O20, toward the central positions and reduce the difference between five and fourfold environment of Ta atoms. The energy difference between non-relaxed and relaxed crystals is 0.1 Ryd per unit cell. As a result of relaxation, atomic positions were changed until the forces on each atom were below 0.5 eV/nm.

The calculated band structure is shown in Fig. 9. The top of the valence band is located at Z point of the Brillouin zone and the bottom of the conduction band is slightly shifted from Γ point toward Y point. The calculated bandgap is 2.04 eV which is two times smaller than that obtained from EELS and spectroscopic ellipsometry measurements. This discrepancy is related to DFT method itself which often underestimates the bandgap values. The result for non-relaxed unit cell which have a bandgap of 2.19 eV is close to the relaxed one. Calculation results further show that the valence band is formed by p-orbitals of oxygen and the conduction band is formed with d-orbitals

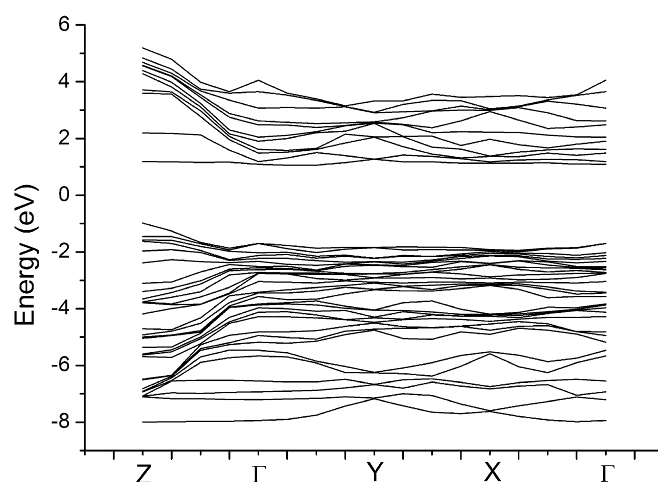

Fig. 9. Band structure of Ta_2O_5 model with relaxed unit cell.

of Ta atoms. Effective masses of electrons and holes were calculated for this band structure. The dispersion law nearby the bottom of conduction band and valence band top are represented with quadratic approximation. As it is seen from Table 3, the effective masses are anisotropic with the lightest masses in z-direction, i.e. perpendicular to Ta–O planes. The calculated electron mass value is comparable with the value $m_e = 0.3m_0$ obtained in [32]. The calculated density of states (DOS) is presented in Fig. 10. As shown in Fig. 10, two additional valence bands formed by Ta 5p states and by O 2s states are found at −36 eV and −20 eV, respectively. As mentioned above the reduction of a difference between five and fourfold environments of

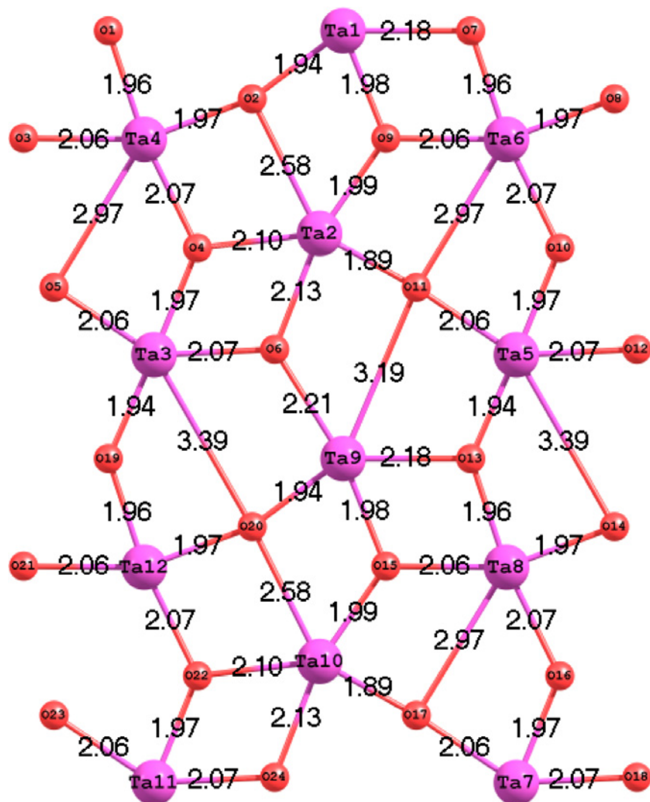

Fig. 8. Fragment of Ta–O plane containing non-relaxed unit cell (Ta1–Ta4 and O1–O6) used in the calculation. Numbers between atoms show distances between them in angstroms.

Table 3
The calculated effective masses of electrons and holes

Particle	m_x	m_y	m_z
Electron	$2.7m_0$	$3.0m_0$	$0.7m_0$
Hole	$2.0m_0$	$0.8m_0$	$0.5m_0$

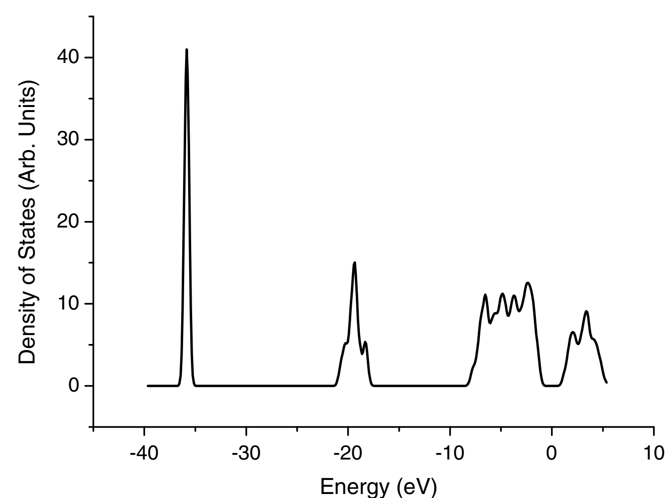

Fig. 10. The density of states of Ta_2O_5. Fermi energy is taken as the reference energy.

Author's personal copy

Ta atoms during relaxation does not lead to significant changes in the band structure. This fact, we believe, permit us to refer the results obtained with present simplified unit cell to real Ta_2O_5 crystal.

7. Charge transport characteristics

Low leakage current is one from the basic requirement for a good dielectric film. Leakage currents through a dielectric are defined by electron and hole injection from the contacts [33–35]. Carrier type in semiconductors can be carried out with Hall effect or thermo power measurement. These methods, however, are not suitable for dielectric materials because of very low density of mobile carriers. Fig. 11 shows the *I–V* characteristics of p-Si/Ta_2O_5/Al structure for two polarities of potential on metal electrode, namely, in enhancement mode (negative potential on Al) and depletion mode (positive potential on Al). In depletion mode and in a dark environment, current saturation is observed with weak current dependence on the voltage applied. The current increases by applying an illumination. Current saturation in depletion mode is governed by the injected minority carriers (electrons) from silicon. In enhancement mode, with negative potential on metal electrode, the current depends exponentially on the applied voltage. In this mode the current is invariant with the illumination effect and practically all applied voltage drops on the dielectric layer.

The schematic energy diagrams for the Si/Ta_2O_5/Al structures without applied potential are depicted in Fig. 12(a) and (d) for p- and n-type silicon, respectively. The value of bandgap energy was taken from the spectroscopic ellipsometry and EELS measurements. The electron energy barrier at the Si/Ta_2O_5 interface is 0.8 eV [36]. Fig. 12 also depicts the energy diagrams of p-Si/Ta_2O_5/Al and n-Si/Ta_2O_5/Al structures under positive (b, e) and negative (c, f) biasing.

In depletion mode, the voltage applied to the p-Si/Ta_2O_5/Al structure is distributed across the dielectric layer and the non-equilibrium depletion layer (Fig. 12(b)). The illumination enhances the rate of minority carrier generation and the thickness of the depletion layer decreases. Consequently, the voltage drop across the depletion layer decreases and the voltage drop across the dielectric layer increases. Thus, the *I–V* characteristics in depletion mode dominate the overall current conduction. Holes flowing from the dielectric into silicon are negligible as compared to the electron current. When negative potential is applied to the metal, the substrate is biased in enhancement mode (Fig. 12(c)) and all the applied voltage drops across the dielectric layer. Under this situation, the electrical conduction in the dielectric material is also provided by the electron injection from the silicon substrate as the electron barrier heights at the Si/Ta_2O_5 and the Al/Ta_2O_5 interfaces are very close (see Fig. 12(a) and (d)).

An alternative behavior of the *I–V* characteristics is found for n-Si/Ta_2O_5/Al structure (Fig. 13). With a positive potential on the metal (i.e. enhancement mode), similar

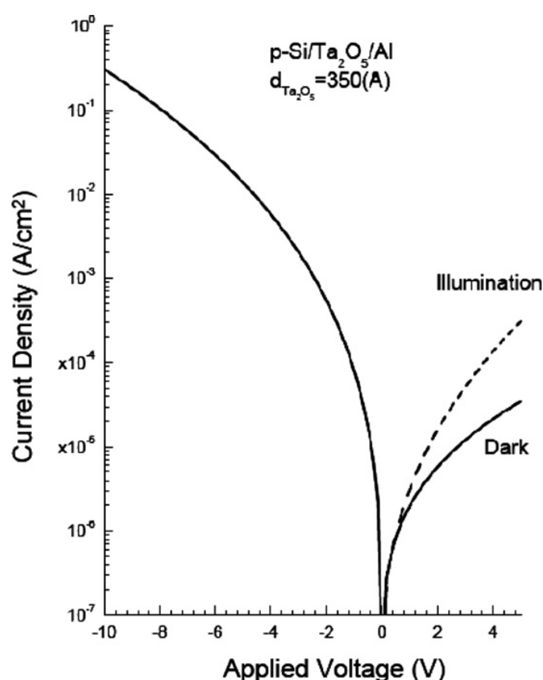

Fig. 11. Current–voltage characteristics for a p-Si/Ta_2O_5/Al structure in the depletion and enhancement modes (solid lines). Points represent the current–voltage characteristics in the depletion mode under illumination.

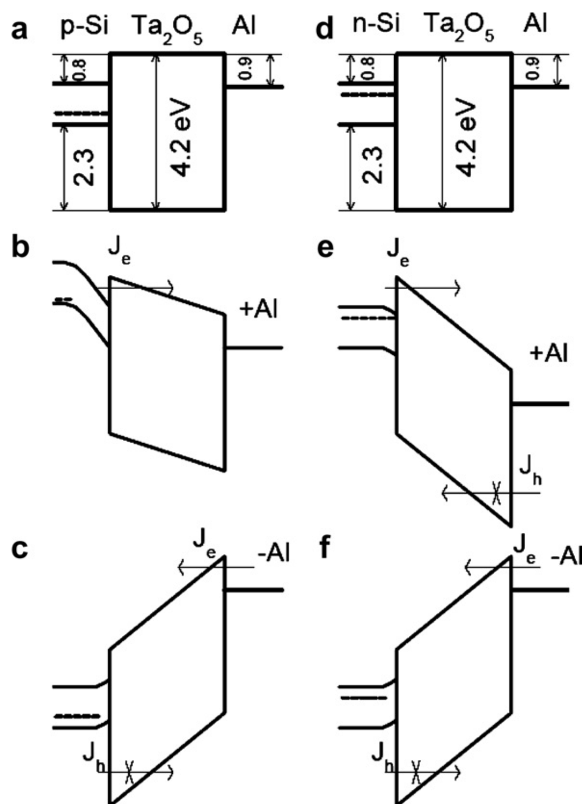

Fig. 12. Schematic energy diagrams for a p-Si/Ta_2O_5/Al (a–c) and an n-Si/Ta_2O_5/Al (d–f) structures. (a, d) Without external applied voltage; (b, f) in the depletion mode; and (c, e) in the enhancement mode.

Author's personal copy

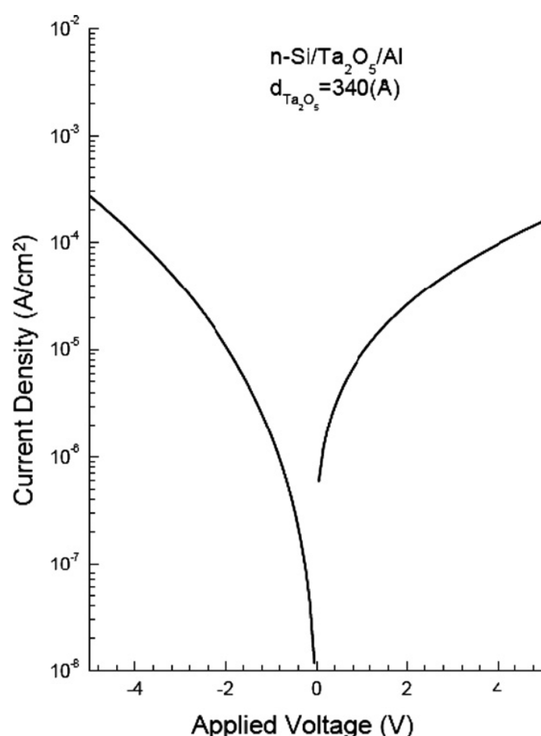

Fig. 13. Current–voltage characteristics for an n-Si/Ta_2O_5/Al structure in the depletion and enhancement modes.

to the p substrate case, all the applied voltage drops across the dielectric layer (Fig. 12(e)). In depletion mode, the *I–V* characteristics reach saturation (Fig. 13). Light illumination does not stimulate the increase of current level; that is, no non-equilibrium depletion layer generated from the injection of holes from the silicon substrate (Fig. 12(f)). The current over the Si/Ta_2O_5 interface is dominated by the electron injection from silicon into dielectric.

Fig. 12 also illustrates the unipolar model of electron current flows in Si/Ta_2O_5/Al structure for two possible polarities of gate bias. As electron traps exist in Ta_2O_5 film [2,37–39], some of the injected electrons will be trapped. The trapped charges may be ionized via either Frenkel or multiphonon mechanism [29,39]. As a result, the current conduction can be enhanced by the trap-assisted conduction process which was also found in ZrO_2 [40,41]. In summary, the current conduction in Si/Ta_2O_5/Al structures is governed by electron current at both potential polarities.

8. Conclusions

Morphology, structure, chemical composition, and optical properties of amorphous tantalum pentoxide (Ta_2O_5) films have been observed. Both optical properties and XPS results confirm that the prepared films are stoichiometric. The variations of refractive index ($\Delta n/n$) and thickness ($\Delta d/d$) are as low as 2.4% and 0.1%, respectively. The surface roughness of the Ta_2O_5 films revealed by AFM measurement is about 0.16 nm. The dispersion of refractive index and extinction coefficient over the spectral range of 1.9–4.9 eV were measured with a spectroscopic ellipsometer. The bandgap energy, determined using reflection spectra, is 4.20 ± 0.05 eV which is further confirmed with electron energy loss spectroscopy measurement. ADF calculations, performed with the ESPRESSO package [42], indicate that the Ta_2O_5 valance band consists of three bands separated by ionic gap. The electron and hole effective masses in crystalline Ta_2O_5 were estimated. The current conduction of Si/Ta_2O_5/Al structure is dominated by electron current.

Acknowledgments

This work was supported by the project 97 of Siberian Branch of Russian Academy of Sciences, RFBR Project 06-02-16621, and a RGC Grant (CityU 121707) of Hong Kong Government.

References

[1] F. Rubio, J.M. Albella, J. Denis, J.M. Martyinez, J. Vac. Sci. Technol. 21 (1982) 1043.
[2] N. Novkovski, E. Atanassova, Appl. Phys. Lett. 86 (2005) 152104.
[3] P.C. Joshi, M.W. Cole, J. Appl. Phys. 86 (1999) 871.
[4] K. Chu, J.P. Chang, M.L. Steigerwald, R.M. Fleming, R.L. Opila, D.V. Lang, R.B. Van Dover, C.D. Jones, J. Appl. Phys. 92 (2002) 308.
[5] H. Wong, H. Iwai, Microelectron. Eng. 83 (2006) 1867.
[6] G.D. Wilk, R.M. Wallace, J.M. Anthony, J. Appl. Phys. 89 (2001) 5243.
[7] V.A. Gritsenko, K.A. Nasyrov, Yu.N. Novikov, A.L. Aseev, S.Y. Yoon, J.-W. Lee, E.-H. Lee, C.W. Kim, Solid State Electron. 47 (2003) 1651.
[8] H. Kimura, J. Mizuki, S. Kamiyama, H. Suzuki, Appl. Phys. Lett. 66 (1995) 2209.
[9] P. Swift, Surf. Interf. Anal. 4 (1982) 47.
[10] V.V. Atuchin, I.E. Kalabin, V.G. Kesler, N.V. Pervukhina, J. Electron. Spectrosc. Relat. Phenom. 142 (2005) 129.
[11] V.V. Atuchin, V.G. Kesler, N.V. Pervukhina, Z. Zhang, J. Electron. Spectrosc. Relat. Phenom. 152 (2006) 18.
[12] V.V. Atuchin, O.A. Alekseeva, V.G. Kesler, L.D. Pokrovsky, N.I. Sorokina, V.I. Voronkova, J. Solid State Chem. 179 (2006) 2349.
[13] V.V. Atuchin, V.G. Kesler, N. Yu. Maklakova, L.D. Pokrovsky, D.V. Sheglov, Eur. Phys. J. B51 (2006) 293.
[14] C.H. An, K. Sugimoto, J. Electrochem. Soc. 141 (1994) 853.
[15] Y. Imai, A. Watanabe, M. Mukaida, K. Osato, T. Tsunoda, T. Kameyama, K. Fukuma, Thin Solid Films 261 (1995) 76.
[16] E. Atanassova, T. Dimitrova, J. Koprinarova, Appl. Surf. Sci. 84 (1995) 193.
[17] E. Atanassova, D. Spassov, Appl. Surf. Sci. 135 (1998) 71.
[18] M. Textor, L. Ruiz, R.F. Hofer, A. Rossi, K. Feldman, G. Hahner, N.D. Spencer, Langmuir 16 (2000) 3257.
[19] S. Chatterjee, S.K. Samanta, C.K. Maiti, J. Phys. D: Appl. Phys. 36 (2003) 901.
[20] W.-J. Chun, A. Ishikawa, H. Fujisawa, T. Tanaka, J.N. Kondo, M. Hara, M. Kawai, Y. Matsumoto, K. Domen, J. Phys. Chem. B 107 (2003) 1798.
[21] E. Atanassova, G. Tyuliev, A. Paskaleva, D. Spassov, K. Kostov, Surf. Sci. Spectra 11 (2004) 1.
[22] R.M.A. Azzam, N.M. Bashara, Ellipsometry and Polarized Light, North Holland, Amsterdam, 1977.
[23] A.V. Rzhanov (Ed.), Fundamentals of Ellipsometry, Nauka, Novosibirsk, 1977 (in Russian).

Author's personal copy

[24] D.E. Aspnes, A.A. Studna, Phys. Rev. B 27 (1983) 985.
[25] H. Arwin, D.E. Aspnes, Thin Solid Films 113 (1984) 101.
[26] J. Tauc, Amorphous and Liquid Semiconductors, Plenum, New York, 1974.
[27] H. Demiryont, J.R. Sites, K. Geib, Appl. Opt. 24 (1985) 490.
[28] J. Robertson, J. Vac. Sci. Technol. B 18 (2000) 1785.
[29] N.C. Stephenson, R.S. Roth, Acta Crystallogr. B 27 (1971) 1037.
[30] H. Sawada, K. Kawakami, J. Appl. Phys. 86 (1999) 956.
[31] R. Ramprasad, M. Sadd, D. Roberts, T. Remmel, M. Raymond, E. Luckowski, S. Karpat, C. Barron, M. Miller, Microelectron. Eng. 69 (2003) 190.
[32] M. Houssa, M. Tuominen, M. Naili, V. Afanas'ev, A. Stesmans, S. Haukka, M.M. Heyns, J. Appl. Phys. 87 (2000) 8615.
[33] V.A. Gritsenko, E.E. Meerson, Yu.N. Morokov, Phys. Rev. B 57 (1997) R2081.
[34] K.A. Nasyrov, Yu.N. Novikov, V.A. Gritsenko, S.Y. Yoon, C.W. Kim, JETP Lett. 77 (2003) 385.
[35] K.A. Nasyrov, V.A. Gritsenko, Yu.N. Novikov, E.-H. Lee, S.Y. Yoon, C.W. Kim, J. Appl. Phys. 96 (2004) 4293.
[36] B.C.-M. Lai, J.-C. Yu, J.Y.-M. Lee, IEEE Electron. Dev. Lett. 22 (2001) 221.
[37] B.C.-M. Lai, N.-H. Kung, J.Y.-M. Lee, J. Appl. Phys. 85 (1999) 4087.
[38] M. Stremme, G.A. Niklasson, M. Ritala, M. Leskela, K. Kukli, J. Appl. Phys. 90 (2001) 4532.
[39] E. Atanassova, N. Novkovski, A. Paskaleva, M. Pecovska-Gjorgjevich, Solid State Electron. 46 (2002) 1887.
[40] T.V. Perevalov, A.V. Shaposhnikov, V.M. Tapilin, K.A. Nasyrov, D.V. Gritsenko, V.A. Gritsenko, in: E. Gusev (Ed.), Defects in High-*k* Gate Dielectric Stacks, Springer, 2006.
[41] D.V. Gritsenko, S.S. Shaimeev, O.P. Pchelyakov, V.A. Gritsenko, JETP Lett. 81 (2005) 587.
[42] S. Baroni, A. Dal Corso, S. de Gironcoli, P. Giannozzi, C. Cavazzoni, G. Balladio, S. Scandolo, G. Chiarotti, P. Focker, A. Pasquarello, K. Laasonen, A. Trave, R. Car, N. Marzari, A. Kokalj, ESPRESSO Technical Report, http://www.pwscf.org/.